A Nanometric Probe of the Local Proton Concentration in Microtubule-Based Biophysical Systems

Aarat P. Kalra, Boden B. Eakins, Sergei I. Vagin, Hui Wang, Sahil D. Patel, Philip Winter, Maral Aminpour, John D. Lewis, Vahid Rezania, Karthik Shankar, Gregory D. Scholes, Jack A. Tuszynski, Bernhard Rieger, Alkiviathes Meldrum

A Nanometric Probe of the Local Proton Concentration in Microtubule-Based Biophysical Systems

Aarat P. Kalra [a], Boden B. Eakins [b], Sergey I. Vagin [c], Hui Wang [d], Sahil D. Patel [e], Philip Winter [f], Maral Aminpour [b, f], John D. Lewis [f], Vahid Rezania [g], Karthik Shankar [b], Gregory D. Scholes [a], Jack A. Tuszynski [d, f, h], Bernhard Rieger [c], Alkiviathes Meldrum [d, *]

[a] Department of Chemistry, Princeton University, Princeton, New Jersey 08544, United States of America

[b] Department of Electrical and Computer Engineering, University of Alberta, 9107–116 St, Edmonton, Alberta T6G 2V4, Canada

[c] Department of Chemistry, Technical University of Munich, Lichtenbergstraße 4, 85747 Garching bei München, Germany

[d] Department of Physics, University of Alberta, 11335 Saskatchewan Dr NW, Edmonton, Alberta T6G 2E1, Canada

[e] Electrical and Computer Engineering Department, University of California, Santa Barbara, California 93106, United States of America

[f] Department of Oncology, University of Alberta, Edmonton, Alberta T6G 1Z2, Canada

[g] Department of Physical Sciences, MacEwan University, Edmonton, Alberta T5J 4S2, Canada

[h] Department of Mechanical and Aerospace Engineering (DIMEAS), Politecnico di Torino, Torino 10129, Italy

Keywords

photonic sensing, fluorescence, double functional, microtubules, biochemical sensor, biological pH

* Corresponding author: ameldrum@ualberta.ca

Abstract

We develop a double-functional fluorescence sensing paradigm that can retrieve nanometric pH information on biological structures. We then use this method to measure the extent of protonic condensation around microtubules, which are protein polymers that play many roles crucial to cell function. While microtubules are believed to have a profound impact on the local cytoplasmic pH, this has been hard to show experimentally due to the limitations of conventional sensing techniques. We show that subtle changes in the local electrochemical surroundings cause a double-functional sensor to transform its spectrum, thus allowing a direct measurement of the protonic concentration at the microtubule surface. Microtubules concentrate protons by as much as one unit on the pH scale, indicating a charge storage role within the cell via the localized ionic condensation. These results confirm the bioelectrical significance of microtubules and reveal a sensing concept that can deliver localized biochemical information on intracellular structures.

Introduction

Microtubules are hollow, cylindrical polymers whose building blocks are the proteins α and β tubulin. They form the mechanical core of axonemes in cilia and flagella[1,2], set up signals for positioning organelles[3,4], present the major part of mitotic spindles that provide the forces required for chromosomal segregation during mitosis[5], and serve as tracks for intracellular macromolecular transport[6,7]. The highly negative electrostatic charge (thought to be ~50*e*) and large dipole moment (3500 – 4000 D depending on the isotype) of the tubulin dimer allow microtubules to acquire electrical properties unexpected for intracellular biomacromolecules[8]. Microtubules act as amplifiers of ionic signals *in vitro*[9,10], may function as intracellular nanowires capable of propagating ionic signals along their length[11,12], are proposed to regulate ciliary 'beating' movement through cationic interactions[13], and appear to control the overall electrochemical character of the intracellular environment[14]. Recent work has shown the critical nature of microtubule-ion interactions in regulating tubulin conformation[15,16], acting as a source of intracellular electrical oscillations[17,18] and operating as ion-selective conduits for charge storage and transport[8]. While nontrivial protonic condensation around a microtubule forms the premise for such roles in intracellular electrical signaling, its magnitude is unknown and its significance is not well understood.

A direct nanometer-scale chemical probe could enable measurement of the pH in the immediate vicinity of a microtubule or any other cellular structure to which such a probe could bind. There is a short history of this idea[19-22], but many efforts were hampered by photodegradation, relatively weak signals in response to pH changes, or detected large pH changes outside of expected biological conditions. Here, we demonstrate direct detection over the important pH range between approximately 6.5 and 7.5, for biological polymers where pH is believed to play a key role within the cellular function. To achieve this, we designed a double-functional fluorescent tag (referred to as NHS-P4VB; see the Experimental section and Fig. 1) that attaches to proteins via the well-known amide bonding through a functional side group. The fluorescence spectrum is highly sensitive to protonation of the pyridine end groups, changing from teal to orange upon full protonation. This label is a special derivative of the main PV4B central backbone we previously developed for wide-gamut lasing applications[23], and here functions both as a fluorescent tag and as a local sensor for protons. Double-functional chromophores such as NHS-P4VB could readily be extended to other intracellular macromolecules and biomarkers,[24] ultimately realizing a method for monitoring biochemical processes on the nanometer scale. We apply this technique to directly infer the degree of proton condensation around a biological polymer and learn how it controls the immediate chemical surroundings. The results have key implications for our understanding of cellular function and show how specially-designed tags can be applied as nanometric chemical probes under biologically meaningful conditions.

Results and discussion

The NHS-P4VB showed a strong fluorescence color shift from teal to orange upon protonation in a DMSO solution (Fig. 1(a,b)), with a concomitant shift in the absorption maxima (see the Experimental section for the synthesis procedure and the Supporting Information for the characterization of NHS-P4VB). These shifts are consistent with the recently described inert version[25], in which the P4VB (chemical structure shown in Fig. 1(c)) evolves through an unprotonated state with a teal fluorescence and an 80% quantum yield, to a monoprotonated state which mainly lowers the quantum yield, and finally to an orange-emitting diprotonated state with a quantum yield of 35%.

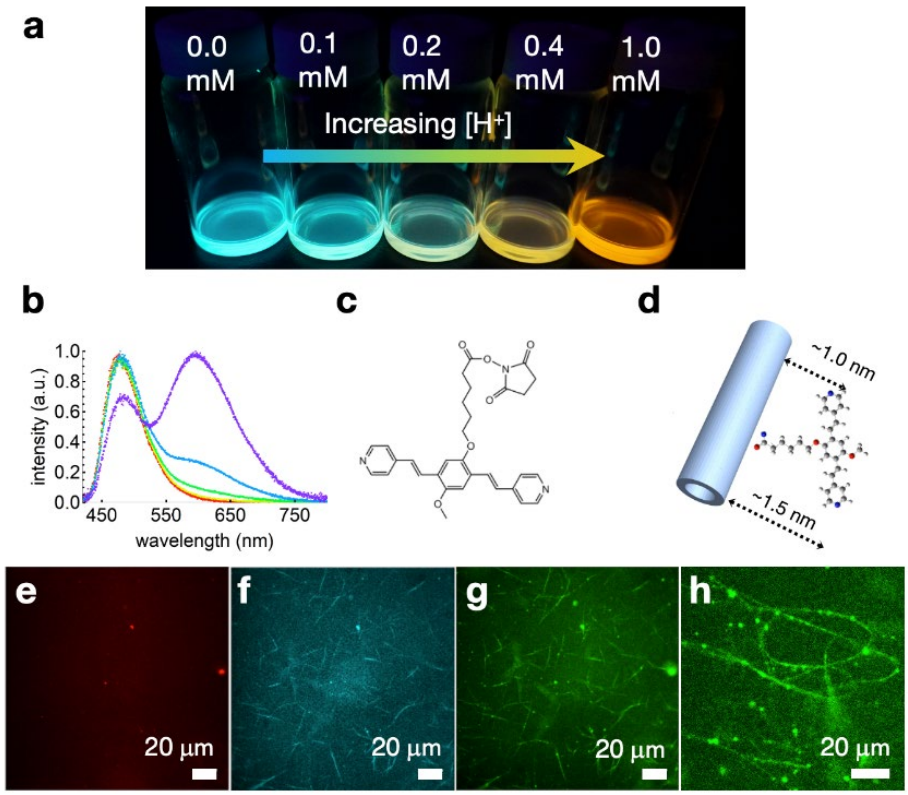

Fig. 1. (a) Blacklight digital photograph showing vials NHS-P4VB (0.01 mM) in DMSO with added HCl concentrations ranging from 0.0 to 1.0 mM; (b) Normalized fluorescence spectra for the same solutions; (c) Chemical structure drawing of NHS-P4VB. The pyridine groups ending the conjugated backbone act as the protonation sites and the N-hydroxysuccinimide (NHS) functional group is on the side-arm; (d) Sketch of a P4VB covalently bound to part of a microtubule (oxygen, nitrogen, carbon, and hydrogen are red, blue, gray, and light gray, respectively; not to scale). The maximal distances from the tubule surface to the two pyridine protonation sites are illustrated in perspective; (e-g) Epifluorescence images of P4VB-labeled microtubules in the red (excitation wavelength: 535 nm; emission wavelength: 610 nm), blue (excitation wavelength: 350 nm; emission

wavelength: 460 nm), and green (excitation wavelength: 480 nm; emission wavelength: 535 nm) channels; (h) A zoom in showing a few microtubules in the green channel. Images e-h are slightly, uniformly, and equally contrast enhanced for visual clarity.

The NHS-P4VB was designed to bind to the lysine components of the tubulin proteins via the well-known amide bonding mechanism, yielding tagged microtubules in a pH8.83 buffer solution (see the Experimental and Supporting Information) that emitted in the blue and green channels (Fig. 1(f-h)) and yielded a visually bluish green or teal-colored fluorescence. While some scattered tubulin aggregates are also apparent in Fig. 1(f), as is common in cases of reconstituted tubulin under various synthesis conditions, the extended thread-like microtubules are clearly visible in all fluorescence images. Based on the NHS-P4VB chemical structure and bonding configuration for a maximally stretched all-trans conformation of the side-arm, the two protonation sites are calculated to be located within a maximum of ~1.5 nm from the microtubule surface (Fig. 1(d)), indicating the approximate range over which the tag will respond to change in the local proton concentration.

The fluorescence spectra of NHS-P4VB (71.60 μM) dissolved in pH8.83 buffer solutions were first recorded as a baseline (referred to henceforth as the solution pH). As the measured solution pH was decreased from 8.83 to 6.47 by the addition of a pH4.8 buffer solution, the fluorescence spectra (Fig. 2(a)) evolved in a similar fashion to those shown in Fig. 1(a,b) for the case of DMSO:HCl. However, the changes here are smaller owing to the narrow range of pH values. While the teal fluorescence intensity decreased, the orange peak emerged as a weak, long-wavelength tail which increased monotonically with decreasing solution pH. At the same time, there was a clear monotonic decrease in the fluorescence intensity, caused by dilution and by the development of the weakly-emissive monoprotonated state of the chromophore.

The same experiments were repeated for a solution containing NHS-P4VB-labeled microtubules (tubulin concentration 3.78 μM), which had been centrifuged to remove any excess chromophore in solution, leaving only the P4VB that was bound to the microtubules. The fluorescence now responded to the local proton concentration up to ~1.5 nm from the microtubule surface (referred to henceforth as the local pH). For the microtubules, the relative intensity in the orange tail was consistently greater than it was for the bulk solution measurements at the same solution pH, implying a lower local pH adjacent to the microtubules as compared to the surrounding medium. The signal, S, was measured as the ratio of the intensities at wavelengths of 495 nm (teal) and 595 nm (orange), respectively (*i.e.*, $S = I_{495}/I_{595}$, where I indicates the relative fluorescence intensity). The approach eliminates interferences from changes associated with photobleaching, dilution, or fluctuations in the pump laser power (as shown in Fig. S1, this ratiometric signal was highly stable). With this definition, the signal is inversely proportional to the degree of protonation of the NHS-P4VB, and is an effective measure of the local proton concentration.

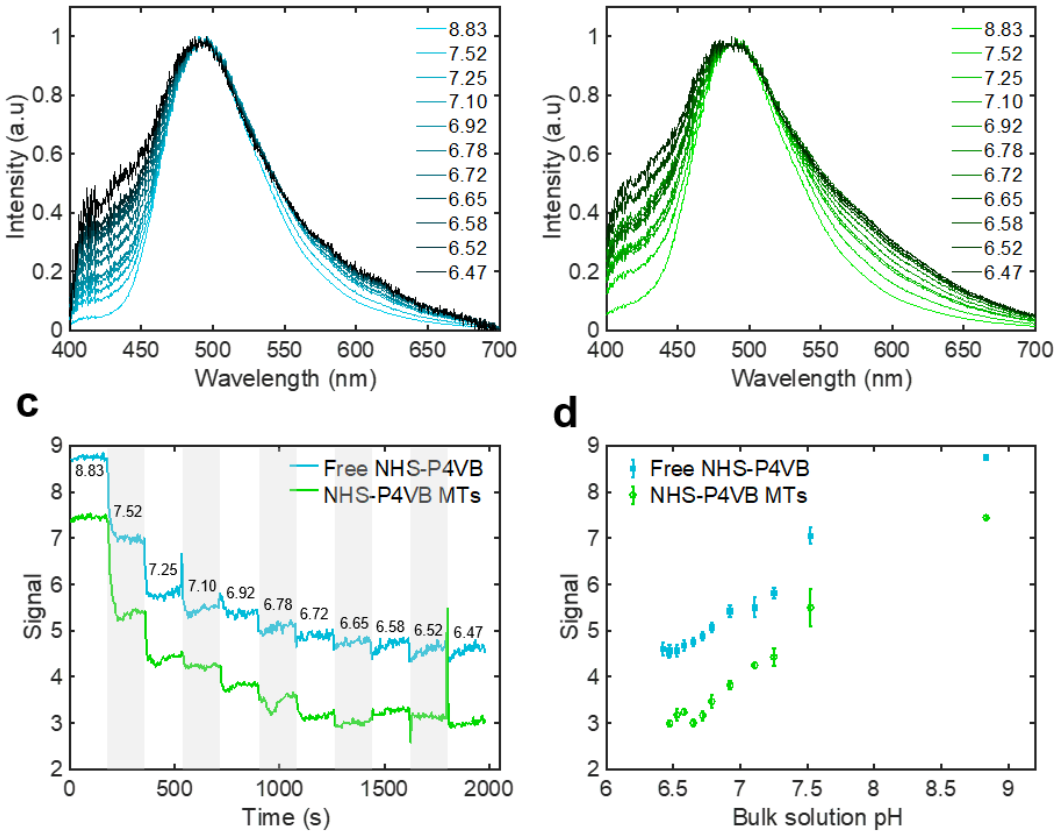

Fig. 2. (a) Normalized fluorescence spectra of NHS-P4VB in buffer solution as a function of the measured solution pH (shown on a color scale). (b) Fluorescence spectra of tubulin conjugated P4VB as a function of buffer solution pH. (c) Variation of the signal (I_{teal}/I_{orange}), plotted as a function of time, as pH4.8 buffer solutions were added in 5 μL steps. (d) The variation of the signals at each step plotted as a function of bulk solution pH value. The error bars represent one standard deviation within each of the steps shown in (c).

The resulting microtubule sensorgram yielded a signal that was clearly and repeatably smaller at every step than it was in the bulk solution (Fig. 2(c)). Some of the noise in the data was found to be related to the physical mixing of small volumes with the pipette tip, which often resulted in sharp noise spikes when the new solution was added (as observed at ~1700 seconds, for example). The step-by-step decrease in the signal was nevertheless observable out to ~1250 seconds. The signal for the microtubules revealed a significantly lower local pH as compared to the solution pH, as shown for every mixing step in the sensorgram. This trend was replicated numerous times (see the Methods and Supporting Information for an evaluation of the errors and uncertainties). The fluorescence spectrum was calibrated by reporting the signal at the measured solution pH, in turn allowing a quantification of the local pH for the bound chromophore within ~1.5 nm of the microtubule surface. A consistently high local proton concentration by about one pH unit in comparison to the bulk solution was observed for all measured conditions (Fig. 2(d)) – clear evidence

of a significant degree of proton concentration by a factor of ~10 in the immediate vicinity of the microtubules. This is the first direct evidence for the attraction of protons to the near-surface region of microtubules in solution.

We next repeated the labeling protocol with several proteins having different charge, including lysozyme (charge at neutral pH = +8*e* from the protein data bank structure code 1GWD), unpolymerized tubulin (–50*e*, code 3RYF), and bovine serum albumin (BSA; –4*e*, code 4F5S) and compared their fluorescence spectra with those from a free NHS-P4VB standard and a reference sample consisting of NHS-P4VB bound to microtubules. We observe that the lysosome signal lies *above* the standard (green line in Fig. 3), consistent with the opposing sign of its electric charge. All the negative-charged proteins lie below the standard, with the BSA (smallest negative charge) being nearest to the standard. The tubulin and microtubules have the most negative charge (-50*e* per dimer) and the resulting ratiometric fluorescence signal is correspondingly the smallest across the entire range of pH (as indicated by the volume of added pH5 solution). Moreover, we also verified that NHS-P4VB conjugated tubulin (polymerized as microtubules) could be cycled through multiple pH-change cycles (Fig. S9).

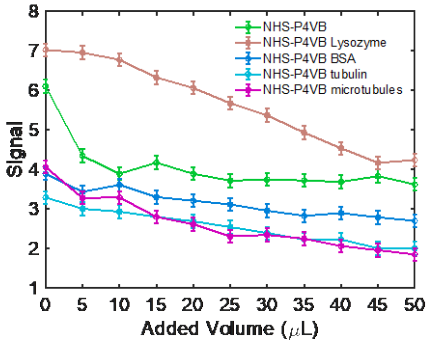

Fig. 3. The ratiometric signal as a function of added volume of MES80 pH5 solution for NHS-P4VB conjugated to various differently-charged proteins. The absolute values of the signal depend on the spectrometer employed to measure it, as expected given the broad nature of the fluorescence spectrum and unavoidable differences in the accuracy of the intensity calibrations among different instruments[26,27].

To validate the experimental results, a microtubule was modeled as an infinite cylinder characterized by a surface charge density and radius with the C-terminus as a separate cylinder connected to the tubule at a right angle. The electric potential was solved by linearizing the Poisson-Boltzmann equation near the microtubule and the C-terminus separately, and subsequently superimposing the potential fields (see the Methods section). Finally, the pH was calculated from the potential by using the Boltzmann equation. Because the local pH is a function of the protein charge, the system was solved iteratively: the pH profiles were calculated for an initial protein charge and then the resultant surface pH was used to determine the protein charge, repeating this process until the solutions converged.

The importance of the C-termini is evident from the calculated local pH values (Fig. 4(a,b)). For distances less than ~1 nm from the surface, the C-termini produce a notably lower local pH owing to their comparatively large negative charge density. The Debye length is estimated to be 7.7 Å in these solutions, which is somewhat less than the expected distance to the NHS-P4VB protonation sites situated at an expected maximum distance of ~1.5 nm from the lysine residues on the tubulin surface. The ability to detect significant changes slightly outside the calculated Debye length suggests that the C-termini extend the ionic double layer surrounding the microtubules outwards in a manner reminiscent of recently-developed electronic biosensors[28,29], further highlighting their significance to the overall electrical character of the microtubules. An increase in the effective thickness of the ionic double layer also enables microtubules to serve as 'ion hoarders' at physiological pH values[9,30,31].

The experimental results are consistent with the pH range calculated from the model (Fig. 4(c)). The data fall mainly within the "C-termini present" band, indicating that the C-termini have a significant net influence on the measured local pH. The finding that microtubules measurably attract protons beyond the Bjerrum length (6.7 Å[30]; the distance at which the Coulombic energy of a point charge is equal to the thermal of energy of the environment) at physiologically relevant pH sheds light on the unusual electrostatic properties of the tubulin dimer. While the convex geometry on the surface of any bio-nanowire increases counterionic condensation, this effect appears exacerbated in the case of microtubules as a result of their C-termini, which have a small surface area in comparison to their Debye volume[28,29].

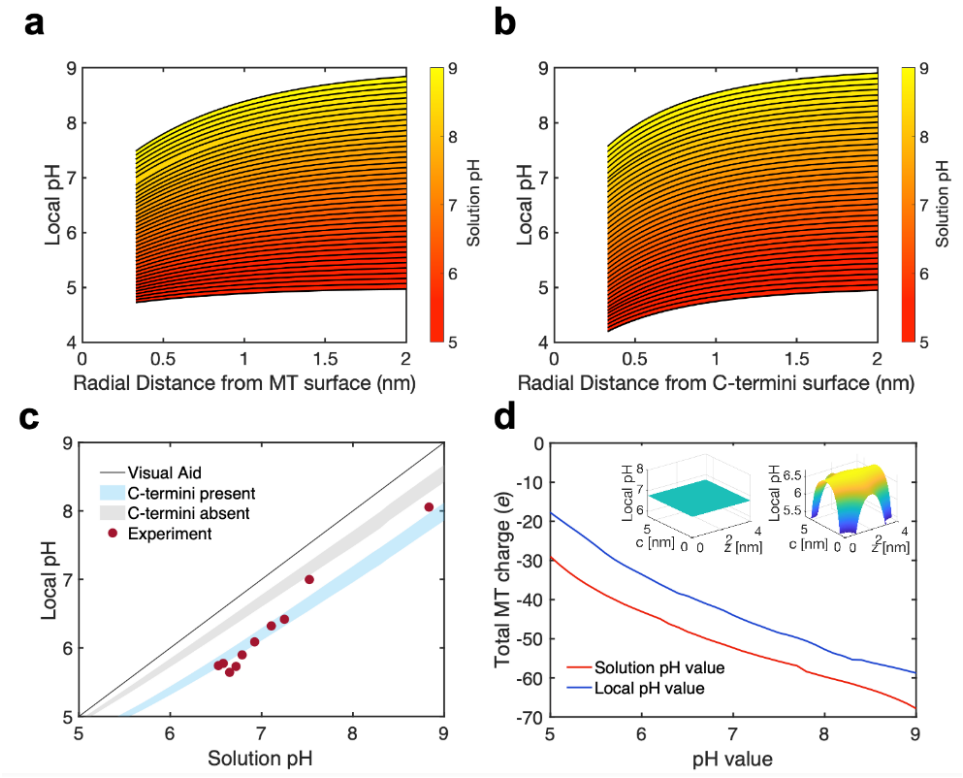

Fig. 4. (a) The local pH calculated as a function of distance from the microtubule surface, for different solution pH values (shaded orange-yellow) with C-termini ignored. The lines show 0.2 local pH contours. (b) the same as in part (a), except that the local pH is calculated with the C-termini present. (c) The local pH as a function of solution pH over a range between 1.0 and 1.5 nm from the microtubule surface (shaded regions). The blue shaded region includes the effect of the C-termini. The experimental data are also plotted (red circles). The errors associated with each point are ~0.06 pH units, which can be derived from the uncertainty of the slope of the calibration values and are close to the size of the data points. (d) The total calculated microtubule charge as a function of the solution pH (orange line) or local pH (blue line). The slight deviations in the lines arise from the specific contributions in the sum of several hundred amino acids in the calculation (see the Methods section). The insets illustrate the local pH profile without the C-termini (left) and with them (right, located at the corners) at a distance of 1.0 Å from the microtubule surface at solution pH7.

The microtubule charge was then calculated as a function of the solution pH, ignoring local pH effects. The base calculation yields a bare tubulin dimer charge of –50*e* at pH7, as previously estimated[32]. However, the experiment shows that the local proton concentration is higher by approximately a factor of 10 as compared to that of the bulk solution. Since the microtubule effectively experiences the local pH, the induced charge required is only –42*e* as opposed to –50*e*. The lowered local pH around a microtubule reveals that their overall charge has been systematically overestimated in previous work which, to our

knowledge without exception, calculates microtubule amino acid charge using the bulk solution pH value. The charge of the tubulin dimer, and its fractional percentage of the total charge on the C-termini, changes with tubulin isotype and additionally depends on post-translational modifications and its animal species source. Thus, while the quantitative results using different tubulin isotypes are expected to vary, our results using a particular tubulin sequence (structure code 3RYF) convey the qualitative impact of the C-termini on the local pH induced by microtubules. The observed trends can be explained by amino acid deprotonation, which leads to the negative surface charge of tubulin at pH7, and increases with pH value[33].

From the biological perspective, the understanding that microtubule-dense regions in living cells (*e.g.* around centrosomes or mitotic spindles, which are crucial for orchestrating mechanical forces during mitosis[5]) have significantly lower pH values as compared to the rest of the cell have several key implications. Our findings show how the microtubules attract protons, measurably lowering the local pH compared to that of the overall surroundings, indicating a charge storage role within the cell *via* cations. The ease of labelling, high microtubule mechanical strength[34, 35] and their high relative stability at room temperature could also allow tagged color-change microtubules to act as powerful tools within a nanodevice (*i.e.*, outside the cell) to map the spatial pH variation in heavily crowded and diverse matrices within nano and microelectrochemical systems[36, 37]. The use of double functional tags in a laboratory setting involving *ex vivo* cancer cell culture could be used to test a panel of drugs and determine their efficacy at various concentrations by quantifying changes in local pH, or to quantify malignancy and disease progression (or regression) for cancer and other metabolic diseases associated with pH perturbations.[38, 39] This work shows how microtubules significantly alter their local chemical environment and highlights the implications that result from this finding.

Conclusion

The ability to perform localized measurements of intracellular pH or other chemical gradients has important implications for the diagnostics and treatment of many types of illness. The intracellular pH is an indicator of the health of the cell; for example, a substantial change in the pH gradient is an adaptive feature in most cancers[40, 41]. Microtubules are believed to control the intracellular proton concentration by lowering the pH of their surroundings and increasing the pH in the cytoplasm. However, nanometric chemical measurements for measuring the local chemical gradients around a microtubule (among other cellular structures) have remained elusive. In this work, we developed a novel nanometric chemical probe that can successfully quantify the local pH within a few bond lengths from the surface of the microtubules. This method could easily be extended to measure the local intracellular biochemistry in a wide range of other structures, with the potential to significantly increase our understanding of cell structure and function.

To achieve these objectives, we developed a "double-functional" fluorescent tag to measure the local pH at biologically relevant conditions not far from pH7. One functionality permits easy covalent binding to any amine group on the target protein, while the second responds to the local chemical changes (in this case via protonation) by sensitively shifting the emission wavelength of the tag. We could thus measure the local pH around the microtubules at distances corresponding to the bond-length separation between the main protonation sites and the protein itself, which in the present case was up to ~1.5 nm. Within this distance, just outside the calculated Bjerrum length, the local proton concentration increased by a factor of ~10 as a result of the highly negative microtubule charge exerting an attractive Coulomb force on positively charged ionic species. The resultant microtubule C-termini charge is significantly less negative than previously believed, owing to the observed condensation of protons in the near-surface region. These results could have significant impact on the understanding of microtubule function and could potentially lead to new approaches for treatment in cases where local intracellular pH is a key indicator of disease.

Methods

Tubulin-P4VB conjugation and microtubule polymerization. The NHS-P4VB was prepared by modifying a procedure described previously[23], as described fully in the Supporting Information. 5 μL of 45.45 μM tubulin was incubated in a 37 °C water bath for 30 minutes to allow microtubule formation and polymerization (Fig. S4). 5 μL of MES80T pH 10 buffer solution (MES80 supplemented with 100 μM taxol; Cytoskeleton Inc, Denver, CO, USA; TXD01) and 1 μL of 4.29 mM NHS-c-P4VB was added to this solution, to allow P4VB-tubulin conjugation of pH 8.5 in the presence of 45.45 μM taxol to ensure microtubule depolymerization did not occur due to the somewhat high solution pH value. This solution was centrifuged (17,000*g*, 20 minutes) and re-suspended with MES80T pH8 buffer to remove unpolymerized tubulin and unbound NHS-P4VB. DLS experiments were performed on the resulting solutions, indicating a significant narrowing of the size distribution after centrifugation (Fig. S5).

Fluorescence spectroscopy. The fluorescence was excited with the combined 352 and 364 nm lines of a UV-optimized Ar^+ ion laser. The laser beam (~5 mW, 4 mm^2 Gaussian beam) was incident on a microcuvette filled with solution (either the blank or the labeled microtubules prepared as described above). The fluorescence spectrum was collected using an intensity-calibrated Ocean Optics USB 2000+ miniature spectrometer. MES80T pH4.8 buffer was added in 5 μL increments every 3 minutes to the 60 μL starting solutions. The micropipette tip was used to gently mix the solutions in each step, before being retracted.

Epifluorescence microscopy. Microscopy was performed using a Zeiss Examiner Z1 microscope equipped with a Zeiss plan-Apochromat 1.4 NA 63x objective lens and a Hamamatsu EMCCD C9100 camera. 2µL solutions of microtubules polymerized using P4VB-labeled tubulin was pipetted onto a glass slide (VWR 48382-173) and a coverslip (VWR 48393-070) was placed on top.

Acknowledgements

This research was funded by grants from NSERC (Canada) awarded to J.A.T. and K.S. and A.M., and by support from Novocure (Haifa, Israel). S.V. and B.R. thank the Deutsche Forschungsgemeinschaft (DFG) for support of the IRTG 2022 ATUMS (project number 245845833) and NSERC (CREATE grant 463990-2015). A.P.K. and B.B.E. thank Alberta Innovates for scholarship support. ToC art by Tomas Spasiuk. A.P.K dedicates this work to his father, Prof. Prem Kumar Kalra.

Data Availability

The authors declare that the data supporting the findings of this study are available within the paper and its Supplementary Information files, as well as from the corresponding author upon reasonable request.

Correspondence should be mailed to A.M. (ameldrum@ualberta.ca)

References

1. Nachury, M. V.; Mick, D. U., Establishing and Regulating the Composition of Cilia for Signal Transduction. *Nature Reviews Molecular Cell Biology* **2019,** *20* (7), 389-405.
2. Ichikawa, M.; Bui, K. H., Microtubule Inner Proteins: A Meshwork of Luminal Proteins Stabilizing the Doublet Microtubule. *BioEssays* **2018,** *40* (3), 1700209.
3. de Forges, H.; Bouissou, A.; Perez, F., Interplay Between Microtubule Dynamics and Intracellular Organization. *The international journal of biochemistry & cell biology* **2012,** *44* (2), 266-274.
4. Kapitein, L. C.; Hoogenraad, C. C., Building the Neuronal Microtubule Cytoskeleton. *Neuron* **2015,** *87* (3), 492-506.
5. Tanaka, T. U., Kinetochore–Microtubule Interactions: Steps Towards Bi-Orientation. *The EMBO journal* **2010,** *29* (24), 4070-4082.
6. Hirokawa, N.; Niwa, S.; Tanaka, Y., Molecular Motors in Neurons: Transport Mechanisms and Roles in Brain Function, Development, and Disease. *Neuron* **2010,** *68* (4), 610-638.
7. Maday, S.; Twelvetrees, A. E.; Moughamian, A. J.; Holzbaur, E. L., Axonal Transport: Cargo-Specific Mechanisms of Motility and Regulation. *Neuron* **2014,** *84* (2), 292-309.
8. Kalra, A. P.; Eakins, B. B.; Patel, S. D.; Ciniero, G.; Rezania, V.; Shankar, K.; Tuszynski, J. A., All Wired Up: An Exploration of the Electrical Properties of Microtubules and Tubulin. *ACS Nano* **2020,** *14* (12), 16301-16320.

9. Priel, A.; Tuszyński, J., A Nonlinear Cable-Like Model of Amplified Ionic Wave Propagation along Microtubules. *EPL (Europhysics Letters)* **2008,** *83* (6), 68004.
10. Priel, A.; Ramos, A. J.; Tuszynski, J. A.; Cantiello, H. F., A Biopolymer Transistor: Electrical Amplification by Microtubules. *Biophysical journal* **2006,** *90* (12), 4639-4643.
11. Sekulić, D.; Satarić, M. V., An Improved Nanoscale Transmission Line Model of Microtubule: The Effect of Nonlinearity on the Propagation of Electrical Signals. *Facta Universitatis, Series: Electronics and Energetics* **2014,** *28* (1), 133-142.
12. Sekulić, D. L.; Satarić, M. V., Microtubule as Nanobioelectronic Nonlinear Circuit. *Serbian Journal of Electrical Engineering* **2012,** *9* (1), 107-119.
13. Satarić, M. V.; Nemeš, T.; Sekulić, D.; Tuszynski, J. A., How Signals of Calcium Ions Initiate the Beats of Cilia and Flagella. *Biosystems* **2019,** *182*, 42-51.
14. Kalra, A. P.; Patel, S. D.; Bhuiyan, A. F.; Preto, J.; Scheuer, K. G.; Mohammed, U.; Lewis, J. D.; Rezania, V.; Shankar, K.; Tuszynski, J. A., Investigation of the Electrical Properties of Microtubule Ensembles under Cell-Like Conditions. *Nanomaterials* **2020,** *10* (2), 265.
15. Chafai, D. E.; Sulimenko, V.; Havelka, D.; Kubínová, L.; Dráber, P.; Cifra, M., Reversible and Irreversible Modulation of Tubulin Self-Assembly by Intense Nanosecond Pulsed Electric Fields. *Advanced Materials* **2019,** *31* (39), 1903636.
16. Chafai, D. E.; Vostárek, F.; Dráberová, E.; Havelka, D.; Arnaud-Cormos, D.; Leveque, P.; Janáček, J.; Kubínová, L.; Cifra, M.; Dráber, P., Microtubule Cytoskeleton Remodeling by Nanosecond Pulsed Electric Fields. *Advanced Biosystems* **2020**, 2000070.
17. del Rocío Cantero, M.; Gutierrez, B. C.; Cantiello, H. F., Actin Filaments Modulate Electrical Activity of Brain Microtubule Protein Two-Dimensional Sheets. *Cytoskeleton* **2020,** *77* (3-4), 167-177.
18. del Rocío Cantero, M.; Etchegoyen, C. V.; Perez, P. L.; Scarinci, N.; Cantiello, H. F., Bundles of Brain Microtubules Generate Electrical Oscillations. *Scientific reports* **2018,** *8* (1), 11899.
19. Eakins, B. B.; Patel, S. D.; Kalra, A. P.; Rezania, V.; Shankar, K.; Tuszynski, J. A., Modeling Microtubule Counterion Distributions and Conductivity Using the Poisson-Boltzmann Equation. *Frontiers in Molecular Biosciences* **2021,** *8* (150).
20. Hilderbrand, S. A.; Kelly, K. A.; Niedre, M.; Weissleder, R., Near Infrared Fluorescence-Based Bacteriophage Particles for Ratiometric pH Imaging. *Bioconjugate Chemistry* **2008,** *19* (8), 1635-1639.
21. Urano, Y.; Asanuma, D.; Hama, Y.; Koyama, Y.; Barrett, T.; Kamiya, M.; Nagano, T.; Watanabe, T.; Hasegawa, A.; Choyke, P. L.; Kobayashi, H., Selective molecular imaging of viable cancer cells with pH-activatable fluorescence probes. *Nat. Med.* **2009,** *15* (1), 104-9.
22. Wang, R.; Yu, C.; Yu, F.; Chen, L.; Yu, C., Molecular fluorescent probes for monitoring pH changes in living cells. *TrAC, Trends Anal. Chem.* **2010,** *29* (9), 1004-1013.
23. Lane, S.; Vagin, S.; Wang, H.; Heinz, W. R.; Morrish, W.; Zhao, Y.; Rieger, B.; Meldrum, A., Wide-gamut lasing from a single organic chromophore. *Light Sci Appl* **2018,** *7*, 101.
24. Saminathan, A.; Devany, J.; Veetil, A. T.; Suresh, B.; Pillai, K. S.; Schwake, M.; Krishnan, Y., A DNA-based voltmeter for organelles. *Nature Nanotechnology* **2021,** *16* (1), 96-103.
25. Wang, H.; Vagin, S. I.; Lane, S.; Lin, W.; Shyta, V.; Heinz, W. R.; Van Dyck, C.; Bergren, A. J.; Gardner, K.; Rieger, B.; Meldrum, A., Metal–Organic Framework with Color-Switching and Strongly Polarized Emission. *Chem. Mater.* **2019,** *31* (15), 5816-5823.

26. DeRose, P. C.; Resch-Genger, U., Recommendations for fluorescence instrument qualification: the new ASTM Standard Guide. *Analytical chemistry* **2010,** *82* (5), 2129-2133.
27. Resch-Genger, U.; DeRose, P. C., Fluorescence standards: Classification, terminology, and recommendations on their selection, use, and production (IUPAC Technical Report). *Pure and applied chemistry* **2010,** *82* (12), 2315-2335.
28. Kesler, V.; Murmann, B.; Soh, H. T., Going beyond the Debye Length: Overcoming Charge Screening Limitations in Next-Generation Bioelectronic Sensors. *ACS Nano* **2020,** *14* (12), 16194-16201.
29. Shoorideh, K.; Chui, C. O., On the origin of enhanced sensitivity in nanoscale FET-based biosensors. *Proceedings of the National Academy of Sciences* **2014,** *111* (14), 5111-5116.
30. Satarić, M.; Ilić, D.; Ralević, N.; Tuszynski, J. A., A Nonlinear Model of Ionic Wave Propagation along Microtubules. *European biophysics journal* **2009,** *38* (5), 637-647.
31. Priel, A.; Tuszynski, J. A.; Woolf, N. J., Transitions in microtubule C-termini conformations as a possible dendritic signaling phenomenon. *European Biophysics Journal* **2005,** *35* (1), 40-52.
32. Van den Heuvel, M.; De Graaff, M.; Lemay, S.; Dekker, C., Electrophoresis of Individual Microtubules in Microchannels. *Proceedings of the National Academy of Sciences* **2007,** *104* (19), 7770-7775.
33. Kalra, A. P.; Patel, S. D.; Eakins, B. B.; Riddell, S.; Kumar, P.; Winter, P.; Preto, J.; Carlson, K. W.; Lewis, J. D.; Rezania, V.; Tuszyński, J. A.; Shankar, K., Revealing and Attenuating the Electrostatic Properties of Tubulin and Its Polymers. *Small* **2020,** *n/a* (n/a), 2003560.
34. Gittes, F.; Mickey, B.; Nettleton, J.; Howard, J., Flexural Rigidity of Microtubules and Actin Filaments Measured from Thermal Fluctuations in Shape. *The Journal of Cell Biology* **1993,** *120* (4), 923-934.
35. Hawkins, T.; Mirigian, M.; Selcuk Yasar, M.; Ross, J. L., Mechanics of microtubules. *J. Biomech.* **2010,** *43* (1), 23-30.
36. Spijkman, M.-J.; Brondijk, J. J.; Geuns, T. C. T.; Smits, E. C. P.; Cramer, T.; Zerbetto, F.; Stoliar, P.; Biscarini, F.; Blom, P. W. M.; de Leeuw, D. M., Dual-Gate Organic Field-Effect Transistors as Potentiometric Sensors in Aqueous Solution. *Adv. Funct. Mater.* **2010,** *20* (6), 898-905.
37. Zhang, Q.; Leonardi, F.; Pfattner, R.; Mas-Torrent, M., A Solid-State Aqueous Electrolyte-Gated Field-Effect Transistor as a Low-Voltage Operation Pressure-Sensitive Platform. *Advanced Materials Interfaces* **2019,** *6* (16), 1900719.
38. Rietman, E. A.; Friesen, D. E.; Hahnfeldt, P.; Gatenby, R.; Hlatky, L.; Tuszynski, J. A., An integrated multidisciplinary model describing initiation of cancer and the Warburg hypothesis. *Theoretical Biology and Medical Modelling* **2013,** *10* (1), 1-19.
39. Fraser, P. E.; Nguyen, J. T.; Surewicz, W. K.; Kirschner, D. A., pH-dependent structural transitions of Alzheimer amyloid peptides. *Biophysical journal* **1991,** *60* (5), 1190-1201.
40. Hao, G.; Xu, Z. P.; Li, L., Manipulating extracellular tumour pH: an effective target for cancer therapy. *RSC advances* **2018,** *8* (39), 22182-22192.
41. Hanahan, D.; Weinberg, R. A., The hallmarks of cancer. *cell* **2000,** *100* (1), 57-70.